

Full paper

Suppression of surface and Auger recombination by formation and control of radial junction in silicon microwire solar cells



Fei Wu^{a,1}, Hao Lin^{a,b,1}, Zhenhai Yang^b, Mingdun Liao^b, Zilei Wang^b, Zhengping Li^a, Pingqi Gao^{b,*}, Jichun Ye^b, Wenzhong Shen^{a,*}

^a Institute of Solar Energy, and Key Laboratory of Artificial Structures and Quantum Control (Ministry of Education), School of Physics and Astronomy, Shanghai Jiao Tong University, 800 Dong Chuan Road, Shanghai 200240, PR China

^b Ningbo Institute of Material Technology and Engineering, Chinese Academy of Sciences (CAS), Ningbo City 315201, PR China

ARTICLE INFO

Keywords:

Radial junction
Micropencil array
Surface recombination
Auger recombination
Black silicon solar cells

ABSTRACT

Black silicon (b-Si) with nanotextures is a promising light-trapping scheme for potentially achieving high conversion efficiency at reduced manufacturing cost in crystalline-silicon solar cells. However, the inherently high aspect-ratio and tiny feature size of the nanostructures are subject to severe surface (large surface areas) and Auger recombination (worse doping profile). These will abate the cost values of b-Si since one has to adopt a comprise strategy of applying shallow nanotextures with antireflection and passivation layers. Here, we show that silicon microwire solar cells featuring well-defined radial junctions can extensively suppress both surface and Auger recombination by providing excellent all-around electrical field. The radially doped silicon micro-pillar devices even show an internal quantum efficiency as good as that of planar substrate and their measured minority carrier lifetimes become nearly independent of total surface area. A great reduction in short-circuit current density loss was further identified as the junction abruptly changed from a fully diffused to a core-shell configuration, manifesting the powerful effectiveness of radial p-n⁺ junction on the suppression of Auger recombination. Furthermore, silicon microwire solar cell with a radial junction demonstrates 37% increase in efficiency compared with the reference cell, suggesting a feasible strategy towards high-efficiency solar devices.

1. Introduction

Black silicon (b-Si) that employs sub-wavelength surface nanotexturing is a very effective way of eliminating front-surface reflection in solar cells without the need of additional antireflection coating [1,2]. In addition, b-Si can be fabricated by cost-effective methods, such as metal-assisted etching and laser modification. So applying b-Si in Si solar cells could be an ideal strategy to boost efficiency as well as to reduce the manufacturing cost. However, the implementation of b-Si in a front-junction solar cell is inherently associated with problems, i.e., larger parasitic surface areas, worse doping profiles (heavily diffused throughout the entire depth of the nanotextures), leading to parallel recombination channels in the emitter: surface and Auger recombination [3,4]. Oh et al. [5] have thoroughly examined the influences of these two recombination channels on the performance of b-Si solar cells and drawn two key points towards high efficiency: keeping shallow depth and moderate doping level. Since then, these golden-rules have always been strictly obeyed by both fundamental researchers and

industrial engineers, irrespective of the sacrifices in light-trapping property due to the adoption of shallow nanotextures (300–400 nm) [6]. The insufficient short-circuit current density (J_{sc}) resulted in unsatisfied efficiencies of below 18%. Additional antireflection layer (SiN_x) was then still needed to boost the efficiency beyond 20%. Subsequent breakthrough came from Savin et al. [7] where they demonstrated a conformal Al₂O₃ coating can provide excellent chemical and electrical passivation to the b-Si nanotextures. Relying on the ultralow surface recombination velocity ($S_{eff} \sim 20 \text{ cm s}^{-1}$) endowed by an 80 nm Al₂O₃ film on a b-Si surface (dual functions with passivation and anti-reflection), extremely high efficiency above 22% was resulted based on an interdigitated back-contacted (IBC) cell. Nevertheless, the Auger recombination in b-Si that was perfectly surmounted in IBC cells, is still an unsurpassed issue in conventional front-junction solar cells where highly-doped emitter must be formed upon the nanotextures.

In contrast to nanotextures, vertically aligned microwires with well-defined diameters and pitches are particularly attractive for achieving high-performance solar cells due to the excellent light-trapping property

* Corresponding authors.

E-mail addresses: gaopingqi@nimte.ac.cn (P. Gao), wzshen@sjtu.edu.cn (W. Shen).

¹ These authors contributed equally to this work.

as well as the capability of forming radially core-shell p-n⁺ junctions [8]. By well adjusting the size of the microwire arrays and the parameters of the diffusion process, a radial emitter with junction depth (~500 nm) and sheet resistance (< 100 Ω sq⁻²) both similar to that of the state-of-the-art planar Si solar cells could be formed [9–11]. Efficient carrier collection and mitigated Auger recombination are therefore highly expected in the core-shell junction configuration, because of a short pathway and a surrounding electrical field with controllable strength [12]. Moreover, silicon microwire solar cell may offer an ideal platform for the development of efficient solar-to-fuel device, a concept of directly turning solar energy into storable fuel [13,14]. The unique features favorable for solar-to-fuel devices consist (1) the sidewalls of microwires provide a large surface area for abundant loading of catalysts, (2) radial junction geometry results in accelerated electron transport between catalysts and silicon absorber. However, by now how the dimensions including height, width, and pitch of microwires, associated with doping temperatures, affect the core-shell junction geometry has not been fully explored. A fundamental understanding of the junction depth and doping level on the surface and Auger recombination losses has rarely been quantified. This leads to poor control and optimization on the aspects of the design and fabrication of radial junction silicon microwire solar cells, hindering their applications in both photovoltaics and solar-to-fuel devices since the unsatisfied efficiencies.

Actually, pencil-like Si nanotexture (nanopencil) arrays with averaged reflectivity below 5% have been demonstrated by our group utilizing a facile wet-chemistry fabrication scheme [15,16]. We previously applied this nanopencil structure in b-Si solar cells, but only a poor efficiency of ~10% was achieved because of the abovementioned recombination issues [17]. Relying on similar wet chemical etching process, it is easy to fabricate micro-sized pencil (micropencil) arrays with tunable pitch, diameter and height, rendering us a platform to successfully construct radial junction Si solar cells and study the effects from junction depth and geometric parameters.

In this paper, the electrical performance of radially phosphorus-doped microwire arrays on p-type Si (p-Si) substrates was thoroughly investigated by experiments and simulations, with the variations of height (1–8 μm), diameter (1 and 2 μm) and junction depth (controlled by the diffusion temperature ranging from 800 to 950 °C). We showed that a superior radial p-n⁺ junction can be formed at diffusion temperature of 825 °C, of which the 2.4 μm (pitch) micropillars even showed an internal quantum efficiency (IQE) as good as that of planar substrate. More interestingly, we found that the minority carrier lifetime becomes nearly independent of the total surface areas (changing the micropillars depth from 1 to 8 μm) once a radial junction was formed. As a result, the modified radial p-n⁺ junction solar cell obtained an enhancement of up to 37% in efficiency compared with the fully-doped reference cell. Our findings fully explored the superiorities of radial junctions in suppressing both surface and Auger recombination, which may provide a new direction towards high-efficiency microtextured solar cells and solar-to-fuel cells.

2. Results and discussion

Firstly, we fabricated three-dimensional Si microstructures with two kinds of pitches, 1.2 and 2.4 μm, via an anisotropic wet etching technique (see Methods). Fig. 1(a–f) demonstrated the scanning electron microscopy (SEM) images of as-fabricated micropillar and micropencil arrays with 1.2 μm-pitch, and the corresponding solar spectrum averaged reflectance (R_{AVE}) was shown in Fig. 1g (The samples with 2.4 μm-pitch were shown in Fig. S1). Note that the ratio of diameter/pitch for all the samples was preset as 1/1.2 according to our previous experiences [16], aiming to obtain a better light-trapping effect. While the aspect ratios of height/diameter were changed from 1 to 4. The microstructure arrays have smooth sidewalls and preferable uniformity, thanks to the improvement of the metal catalyst system and etching solution. As illustrated in Fig. 1g, with increasing the height beyond

1 μm, the R_{AVE} of pillar samples kept at a stable value (~11%), due to the strong reflection from the relatively large flat portions on the top [18,19]. In contrast, the R_{AVE} of pencil samples was greatly decreased from 12.5% to 1.6% with the increase of height from 1 to 4 μm, demonstrating more efficient light-trapping properties of tapered configurations [16]. It should be mentioned that the reflection from the basal open area may also become weaker with the increase of pencil height, especially for depth higher than 2 μm. Therefore, the aspect ratio of pencil arrays should be kept over 2 to suppress the reflection below 5%.

The antireflection property is one of important factors for high efficiency solar cells. Surface recombination, which is always relevant to the surface area, is another crucial factor. A^{F} and A_{proj} were defined here to represent the micro-textured front surface area and the corresponding projected area (equal to the planar area of the polished wafer), respectively. The ratio of $A^{\text{F}}/A_{\text{proj}}$ [5] that was labeled on the top edge of Fig. 1g reveals the enhancement of surface area of micro-pillar arrays. For the micropillar, the $A^{\text{F}}/A_{\text{proj}}$ increases from 2.26 to 6.04 with the growth of height from 1 to 4 μm. Here, radial p-n⁺ junctions covered with thermal-grown SiO₂ layers, as schematically shown in the inset of Fig. 1h, were utilized to evaluate the quality of surface passivation. The lifetime measurement gives an effective carrier lifetime (τ_{eff}) including the contributions from both bulk lifetime (τ_{bulk}) and surface lifetime (represented by front and back surface recombination velocity, $S_{\text{eff}}^{\text{F}}$ and $S_{\text{eff}}^{\text{B}}$). That is $1/\tau_{\text{eff}} = 1/\tau_{\text{bulk}} + (S_{\text{eff}}^{\text{F}} + S_{\text{eff}}^{\text{B}})/W$, where W is the wafer thickness. For same batch of p-Si wafers with identical rear-surface configurations (planar surface coated with SiO₂), the change in τ_{eff} therefore mainly reflected the passivation quality of front surface (different microstructures coated with SiO₂). The corresponding τ_{eff} for different front-side designs were collected and shown in Fig. 1(h and i) [7]. It revealed that the five samples in Fig. 1h have similar τ_{eff} in a large span of excess carrier densities (from 10^{14} to 10^{16} cm^{-3}). For a fair comparison, the lifetime of each texture at a universal excess carrier density ($1 \times 10^{15} \text{ cm}^{-3}$) was extracted and shown in Fig. 1i. Surprisingly, the effective lifetime of the micropillar samples are nearly independent of the area ratios of $A^{\text{F}}/A_{\text{proj}}$ and even comparable to the values from planar and pyramidal samples. According to the equation of $S_{\text{eff}}^{\text{F}} = S_{\text{loc}}^{\text{F}} \cdot A^{\text{F}}/A_{\text{proj}}$, surface recombination should largely depend on surface area, where $S_{\text{loc}}^{\text{F}}$ is the local effective surface recombination velocity at the front surface [5]. Therefore, the less difference of τ_{eff} for different $A^{\text{F}}/A_{\text{proj}}$ indicates that the surface recombination should become a secondary factor. For example, assuming $S_{\text{loc}}^{\text{F}} = 1 \text{ cm/s}$ and $\tau_{\text{bulk}} = 250 \mu\text{s}$ for our wafer ($W = 400 \mu\text{m}$), $\tau_{\text{eff}} = 248$ and $241 \mu\text{s}$ can be calculated for planar ($A^{\text{F}}/A_{\text{proj}} = 1$) and pillar 4 ($A^{\text{F}}/A_{\text{proj}} = 6$), respectively. At this situation, with a good surface passivation, the τ_{eff} becomes nearly independent to the surface areas. Therefore, the actually measured lifetime of 202/219 μs for pillar 4/planar indicates a pretty good surface passivation for microstructures. On the other hands, nanowire structure exhibited a remarkable negative relevant relation between the effective lifetime and the area ratio of $A^{\text{F}}/A_{\text{proj}}$, indicating severe surface recombination [5,20]. In reference 5, the effective minority carrier lifetime in SiO₂ passivated b-Si was found rapidly dropped from ~220 to ~110 μs as increasing the $A^{\text{F}}/A_{\text{proj}}$ from 2.9 to 5.2 [5]. This indicates a different passivation mechanism of microstructures compared to that of nanowires, which will be discussed in next section.

Additionally, IQE spectra will give more information of spatially resolved extraction capability on photogenerated carriers. Thus IQE becomes a passivation-quality-dependent parameter indicative of the surface and Auger recombination because of the elimination of effects from light-trapping properties. The Auger recombination from the front n⁺ doped layer can be well evaluated by the IQE spectra at short wavelength range while the surface recombination is relevant to full spectra. As shown in Fig. 2a, the IQE responses of larger pitch (2.4 μm) micropillar that was doped at 850 °C was firstly examined aiming to study the influence of $A^{\text{F}}/A_{\text{proj}}$ on the surface recombination. Note that the purpose of choosing larger pitch and medium doping temperature is

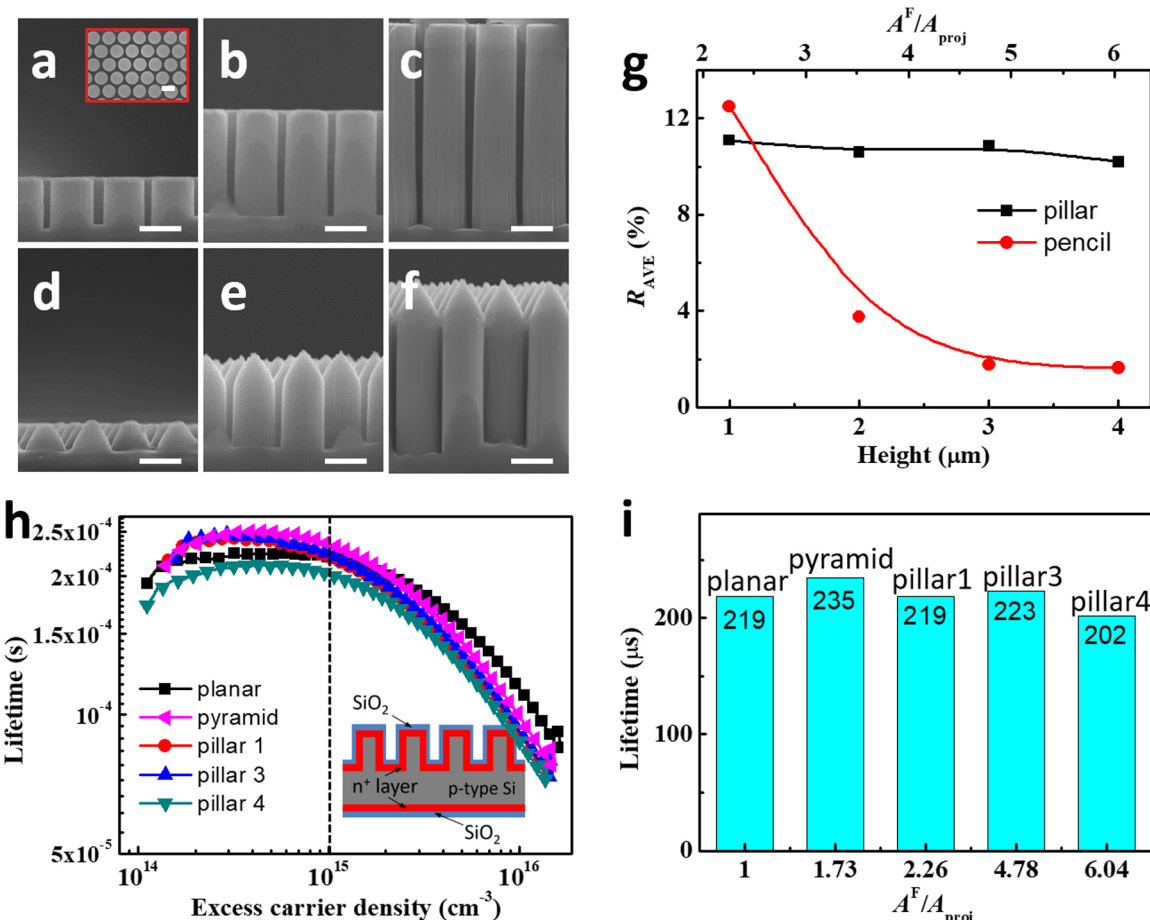


Fig. 1. Cross-sectional SEM images of 1.2 μm-pitch micropillar (a–c) and micropencil (d–f) arrays with a height of 1, 2, and 4 μm, respectively. The inset in (a) shows the top-viewed SEM image of micropillar arrays. (g) The solar spectrum averaged reflectance R_{AVE} of the micropillar (black) and micropencil (red) arrays. (h) The minority carrier lifetime as a function of excess carrier density for different structures. The inset shows the schematic of microtextured wafer with passivated p-n⁺ junctions for lifetime measurements. (i) The lifetime as a function of A^F/A_{proj} at excess carrier density of $1 \times 10^{15} \text{ cm}^{-3}$. Here, A^F/A_{proj} represents for micropillars. All scale bars in SEM images are 1 μm. Pillar 1, 3 and 4 represent the pillars with a height of 1, 3 and 4 μm, respectively. (For interpretation of the references to color in this figure legend, the reader is referred to the web version of this article.)

to largely reduce the influence of Auger recombination (details will be described in Fig. 5). One can see from Fig. 2a that the IQE values of 2.4 μm-pitch micropillars were well maintained with the increase of aspect ratio. This trend coincides with the results of the effective carrier lifetime, indicating that the microwire radial p-n⁺ junction may play a crucial role in the surface passivation. Meanwhile, the IQE spectra in the blue spectrum range (from 400 to 500 nm) even showed a little enhancement as increasing the height from 2 to 8 μm, manifesting a possible superiority of radial p-n⁺ junctions in shortening the length of the carrier collection [21,22].

The influence of doping temperature on the IQE spectra for front configurations with planar substrate, 2.4 μm-pitch micropillars and 1.2 μm-pitch micropillars were further studied and shown in Fig. 2(b–d), respectively. One can clearly find the IQE in blue spectra range for the same structure decreases along with the elevation of doping temperature. More importantly, this decline tendency becomes much prominent with the decrease of structures' pitch (planar counterpart can be considered here as infinite pitch). For example, the IQE value at 400 nm wavelength for the planar device (Fig. 2b) reduced from 100% to 82% as doping temperature increased from 825 °C to 875 °C, while the IQE at same wavelength for the 1.2 μm-pitch micropillars was found decreased from 90% at 825 °C to 22% at 875 °C (Fig. 2d). The reduced IQE mentioned above could be roughly attributed to the deteriorated Auger recombination in the heavy doping region, which would become more serious with the growth of doping

depth and concentration at elevated doping temperature [23]. The abrupt decline in IQE spectra in Fig. 2d may indicate a transformation of the junction configuration in the 1.2 μm-pitch micropillars, i.e. from a core-shell p-n⁺ junction to all ‘dead layer’ structure (heavily diffused throughout the entire depth of the pillars).

Numerical simulations were further implemented to mimic the possible transformation process in junction configurations of 1.2 μm-pitch micropencil structures under different doping temperatures. More information about the simulation can refer the details in the Method of Simulation. To well match with the experimental results, the doping information used in this simulation was extracted from the experimental data and we assumed an ideal case of a uniform doping layer along with the surface of structure. Fig. 3a depicted the dopant concentration as a function of depth for the planar structures at different doping temperatures. According to the experience that Auger recombination commonly predominates the recombination process when the dopant concentration (N_d) exceeds $1 \times 10^{18} \text{ cm}^{-3}$ [24], it is easy to find that the thickness of high Auger recombination layer increases from 0.15 to 1.1 μm as the doping temperatures rise from 800 °C to 950 °C. If considering the $N_d > 1 \times 10^{18} \text{ cm}^{-3}$ as ‘dead layer’, as shown in Fig. 3c, one can clearly see that the all ‘dead layer’ structures of 1.2 μm-pitch micropencil will be formed when the doping temperatures exceed 900 °C.

In order to intuitively state the Auger recombination in the doping process, the profile of the Auger recombination rate was simulated. The

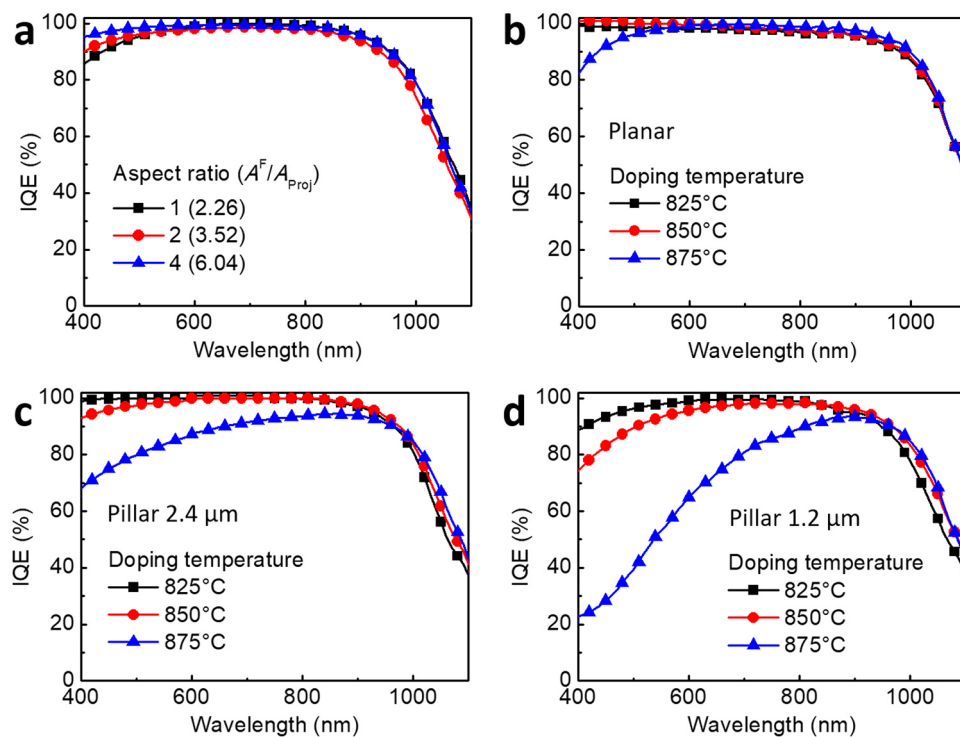


Fig. 2. IQE curves of the silicon micropillar solar cells. (a) 2.4 μm -pitch micropillars with different aspect ratios under 850 °C doping condition. (b) Planar, (c) 2.4 μm -pitch micropillars (with 2/1 aspect ratio) and (d) 1.2 μm -pitch micropillars (with 2/1 aspect ratio) under different doping conditions.

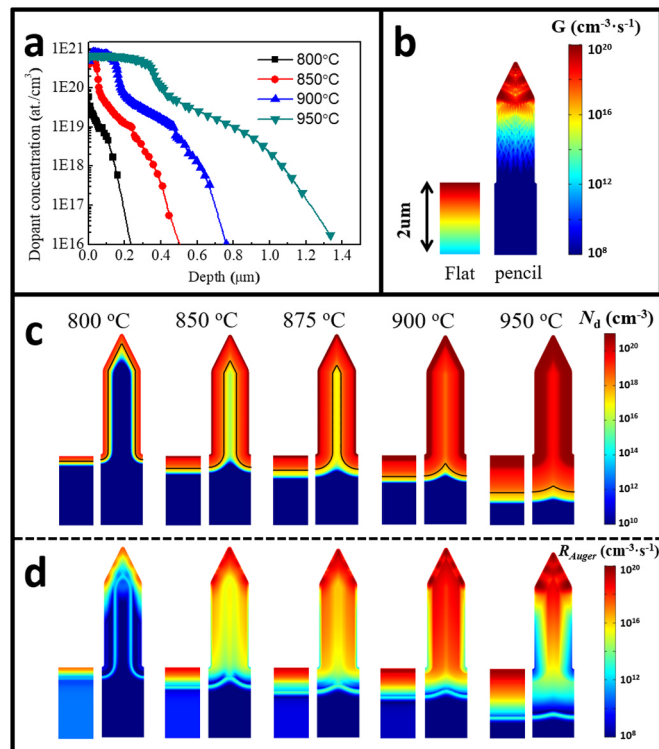


Fig. 3. Analysis of Auger recombination. (a) Electrochemical capacitance-voltage (ECV) profiles of the p-n⁺ junction from planar samples with doping temperature of 800 °C, 850 °C, 900 °C and 950 °C. (b) Simulated distribution profiles of the photogenerated carriers for planar sample and 1.2 μm -pitch micropencil structures at 400 nm wavelength. (c) Simulated doping profiles and (d) corresponding distribution of Auger recombination rate at 400 nm wavelength of planar samples and 1.2 μm -pitch micropencil structures under doping temperature of 800 °C, 850 °C, 875 °C, 900 °C and 950 °C.

net Auger recombination rate is defined by

$$R_{\text{Auger}} = R_{\text{hhe}} + R_{\text{eeh}} = C_p(p^2 n - n_i^2 p_0) + C_n(p n^2 - n_i^2 n_0) \quad (1)$$

where C_p and C_n are the separate Auger coefficients, p_0/n_0 and p/n are the hole/electron densities under thermal equilibrium for the dark and illumination case, respectively, n_i is the intrinsic carrier density. Thus, $n = n_0 + \Delta n$ and $p = p_0 + \Delta n$, where Δn is the excess carrier density, which depends on the photogenerated carriers. As shown in Fig. 3b, we showed the cross-sectional distribution of concentration of photogenerated carriers (G) at $\lambda = 400$ nm for the planar counterpart and 1.2 μm -pitch micropencil. The penetration depth at $\lambda = 400$ nm for the planar sample is $\sim 2 \mu\text{m}$, which means it can well expose the recombination information inside the structure for the pencil sample described above. Since the doping temperatures have a direct effect on the doping concentration (N_d) as shown in Fig. 3a, we then discussed the carriers' distribution under thermal equilibrium. Obviously, with the increase of doping temperatures, heavy-doping region fulfill the structures gradually as shown in Fig. 3c, which maintains high consistency with the measured doping concentration in Fig. 3a. Fig. 3d showed the corresponding cross-sectional distribution of Auger recombination rate (R_{Auger}) for the two structures at $\lambda = 400$ nm. As the doping temperature increased, more photogenerated carriers were involved in 'dead layer', leading to severe Auger recombination.

To help understand the difference between the all 'dead layer' structure and the radial p-n⁺ junction structure in suppressing surface and Auger recombination, schematics of excess carrier recombination mechanisms were proposed in Fig. 4. We directly compared the structures with nano- and micro-dimensions, shown in Fig. 4a and b, respectively. Here we assumed both structures underwent the same doping condition and received a uniform p-n⁺ junction with depth of 150 nm. In this case, the entire nanostructures with the diameter of 200 nm become all 'dead layer' (Fig. 4a), while the microstructures with the diameter of 1 μm can form the core-shell p-n⁺ configuration (Fig. 4b). For nanostucture system, the n⁺ doping layer could fulfill the whole nanostucture region as well as the part of contiguous substrate (red section in Fig. 4a), resulting in an unfavorable energy band bending in the textured

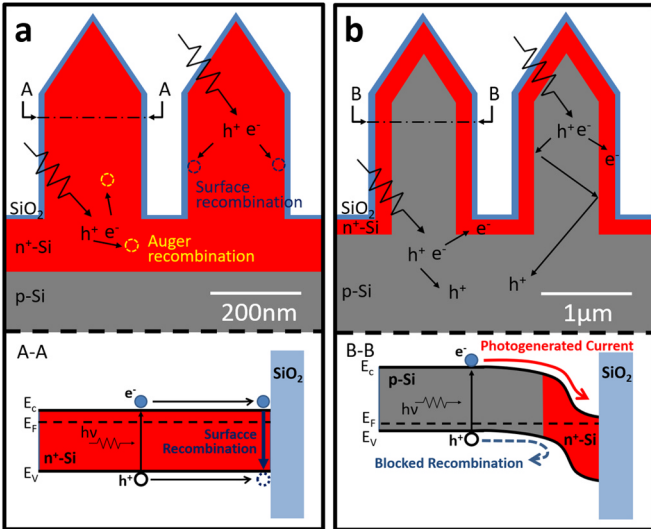


Fig. 4. Schematic of excess carrier recombination mechanisms in two dimensional silicon structures: (a) nano- (b) micro-. (A-A) and (B-B) are the corresponding energy band diagrams of cross profile of nano- and micro-structure, respectively.

Si as shown in Fig. 4A-A and thus facilitating the carriers' recombination including surface and Auger recombination. As to the situation of nanowire, the fully-doped profile can equivalent to a planar structure with deeper diffusion depth and an enlarged surface which is rich in defects. The total diffusion depth equal to the sum of nanowire height and the diffused depth beneath. It is well known that even for the planar structure, the τ_{eff} and J_0 (saturation current density) will also be changed dramatically with the diffusion depth and concentration [25]. The τ_{eff} has a reverse relation with the diffusion depth. Therefore, certainly, the τ_{eff} of nanowire will largely depend on the height of nanowire. However, for the radial p-n junction of microwire, the diffusion layer can be well controlled in a thin layer along with the surface of structure. Due to the quite short distance in the radial direction and the all-around field configuration, the thin radial p-n junction can form a strong field. With the help of this strong electric field, holes will be prevented from the surface and the surface recombination of microstructure will be largely suppressed, as shown in Fig. 4B-B [26]. Meanwhile, because the photo-generated carriers mainly exist in the center of pencil structures (Fig. S2), the Auger recombination can also be well suppressed through keeping the center of pencil structure at a low doping level (p -Si). Therefore,

micropillar with radial p-n junction can maintain good surface passivation (Fig. 1i) and less IQE loss (Fig. 2a) from Auger recombination even for the cases of $A^F/A_{\text{proj}} > 5$.

Except for the discussion on Auger recombination rate at a specific wavelength of 400 nm, the J_{sc} losses across the entire considered wavelengths (i.e., 300–1200 nm) under different doping temperatures were also collected by both simulation and experiments, as shown in Fig. 5(a and b). Because the surface recombination is no longer the main factor that is responsible for J_{sc} loss, we neglect it in this simulation and only consider J_{sc} loss caused by Auger recombination. Fig. 5a illustrated the J_{sc} loss as a function of doping temperatures and the pitches of pencil arrays. For the four samples of planar silicon and 0.6, 1.2, 2.4 μm -pitch micropencil arrays, a similar tendency of increasing J_{sc} loss with the doping temperatures was clearly observed. In addition, at the same doping temperature, the J_{sc} loss become more pronounced with shrinking the feature size from infinite (planar), 2.4–0.6 μm . Region I and Region II were thus defined to represent the micropencil structures with all ‘dead layer’ (similar as Fig. 4a) and core-shell p - n^+ junction (similar as Fig. 4b), respectively. The region definition is based on whether the ‘dead layer’ ($N_d > 1 \times 10^{18} \text{ cm}^{-3}$) depth crosses over the diameter of micropencil or not. For example, the ‘dead layer’ depth of 850 °C doping temperature is about 0.35 μm , which exceeds the radius of 0.6 μm -pitch pencil (0.25 μm), so it belongs to Region I. From Fig. 5a, one can find that micropencil structures have different transformation temperatures from Region II to Region I depending on the different diameters. At the boundary between region I and region II, an abrupt change in J_{sc} loss was identified, indicating the powerful effectiveness of the formation of radial p-n⁺ junction on suppression of the Auger recombination.

To further verify the simulated results, the experimental J_{sc} losses were presented in Fig. 5b. To remit the influences of recombination on the rear side, the experimental J_{sc} losses shown here were calculated by integrating IQE spectrum weighted by photon flux density of AM 1.5 solar spectrum from 300 to 900 nm. The experimental results agreed well with the simulated values. The planar device exhibits minimum J_{sc} loss of below 2 mA/cm² even at a higher doping temperature of 875 °C. As the doping temperature dropped down to 850 °C, the J_{sc} loss of 2.4 μm -pitch and 1.2 μm -pitch micropencils are only 0.5 and 2.1 mA/cm², respectively. However, at the elevated doping temperature of 875 °C, J_{sc} loss from 1.2 μm -pitch micropencils rapidly increased to more than 12 mA/cm² due to the formation of all ‘dead layer’ in the structure (Region I). It is worth mentioning that even though the trends of experiments are similar to that of simulation, the changing temperature of J_{sc} loss from experiments is slightly lower than that from the simulation. This variation may come from the neglect of surface recombination, the assumption of forming uniform p-n⁺ junction [27]. In

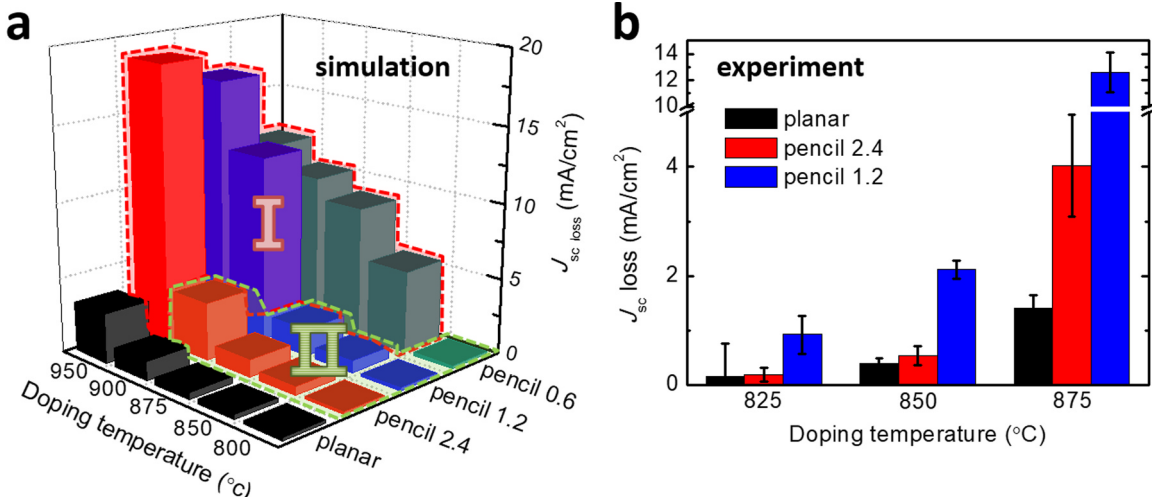


Fig. 5. (a) Simulated and (b) experimental results of J_{sc} loss analysis from the Auger recombination in diffusion layers. Pencil 0.6, pencil 1.2 and pencil 2.4 represent pencil arrays with the pitches of 0.6, 1.2 and 2.4 μm , respectively.

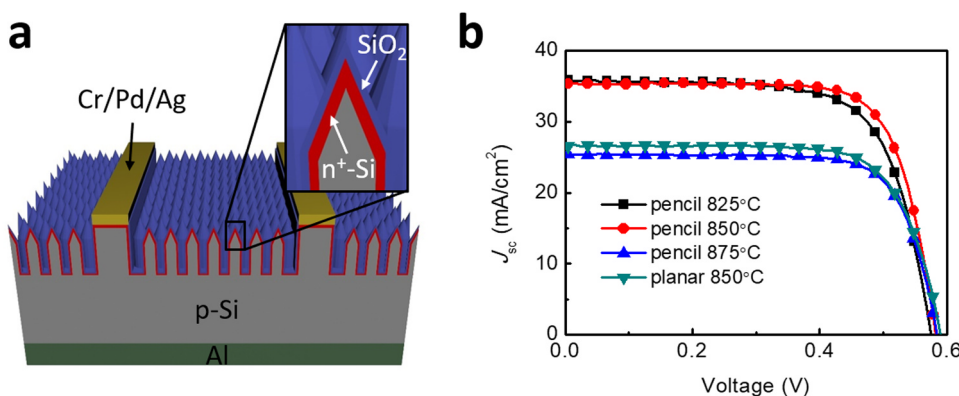


Fig. 6. Photovoltaic performances of solar cells equipped with micropencil arrays under different doping temperatures. (a) Schematic illustration of the silicon micropencil solar cells. (b) J-V curves of planar (reference) and micropencil solar cells. The pitch is 1.2 μm.

fact, for reducing the influence of surface recombination from the surface defect, it is better to form a strong field passivation along with the whole surface of textures. In addition, in order to reduce the influence of Auger recombination, the thickness of the diffusion layer should be controlled as thin as possible. Therefore, the optimized diffusion layer should be uniformly distributed along with the surface of microwire structures. Although it shows a relative uniform doping with an indirect doping method (see details in Fig. S3), improvements in order to form a thin but homogeneous enough diffusion layer should be emphasized in future.

According to above discussion, well-designed micropencil arrays can be a promising platform to render the formation of radial p-n⁺ junction with tunable junction depth. As shown in Fig. 6, silicon micropencil solar cells were therefore fabricated with varied doping temperatures. The schematic of the cells was shown in Fig. 6a. Limited by the immature fabricating techniques including large shaded area (~10%, about 4 mA/cm² loss in J_{sc}) and the high resistance of top metal contacts and poor aluminum back surface field (Al-BSF), the photovoltaic (PV) performances shown here are relatively unsatisfied. Nevertheless, the results showed in Fig. 6b and listed in Table 1 can still give great potential for high-efficiency silicon micropencil solar cells with radial junctions. Note that the J_{sc} of micropencil arrays with 825 °C and 850 °C doping temperatures are both higher than 35 mA/cm², while it rapidly drops down to 25.4 mA/cm² for the 875 °C doping temperature, with a value even less than that of planar counterpart. This phenomenon is consistent with Fig. 5b, indicating the entrance from Region II to Region I (as indicated in Fig. 5a). As a result, our micropencil device achieved the best PCE of 15.3%, with a V_{oc} of 582 mV, a FF of 74.4% and a superior J_{sc} of 35.3 mA/cm² at 850 °C.

3. Conclusion

In summary, silicon microwire solar cells with radial p-n⁺ junctions were successfully fabricated, of which the surface and Auger

recombination, as well as PV performance were systematically studied as a function of the structural parameters and junction depth. Different to the conventionally nanotextured b-Si, the surface passivation qualities of micropillar arrays with radial p-n⁺ junctions are nearly independent to the pillar height (i.e. the aspect ratio), and even comparable to the planar silicon (lifetimes > 200 μs). Further simulated and experimental studies showed that the Auger recombination on the microwire solar cells has a close correlation to the doping condition and the diameter of microstructures. The 2.4 μm-pitch micropencil arrays with a radial p-n⁺ junction formed at 850 °C can suppress the Auger recombination related J_{sc} loss as low as 0.5 mA/cm². As a result, we obtained a champion efficiency of 15.3% for the silicon micropencil solar cells, much higher than that of reference cells with fully-doped emitters (11.1%). Our findings show that the formation and control of radial junction on silicon microwire arrays can efficiently suppress both surface and Auger recombination, indicating a feasible way towards high-efficiency solar cells and solar-to-fuel devices.

4. Methods

4.1. Method of simulation

In this simulation, the COMSOL Multiphysics software was employed to implement the photoelectric simulations, which gain the performances of devices by solving the Maxwell's and carrier transport equations. The periodic boundary conditions were utilized to ensure a perfect cell on the double sides for both optical and electrical modules. In the optical module, by coupling the spatial structure with the frequency domain, we can obtain a series of optical parameters including absorption response and electric field distribution as well as photo-generated carriers' distribution. Then, based on the carriers' generation in the optical module, the electrical processes including carriers' transport, recombination and collection can be well imitated and the stabilized distributions, which includes the carriers and recombination

Table 1
Photovoltaic performances of the silicon solar cells in Fig. 6b.

Samples ^a	V _{oc} ^b (V)	J _{sc} ^b (mA/cm ²)	FF ^b (%)	PCE ^b (%)
Planar (reference)	0.590 (0.588 ± 0.002)	26.6 (26.4 ± 0.3)	72.9 (72.5 ± 0.4)	11.4 (11.3 ± 0.1)
Pencil 825 °C	0.575 (0.574 ± 0.001)	35.7 (35.5 ± 0.2)	70.2 (70.4 ± 0.2)	14.4 (14.4 ± 0.1)
Pencil 850 °C	0.582 (0.584 ± 0.002)	35.3 (35.0 ± 0.5)	74.4 (73.8 ± 0.7)	15.3 (15.1 ± 0.2)
Pencil 875 °C	0.584 (0.582 ± 0.002)	25.4 (25.2 ± 0.7)	74.8 (74.3 ± 1.0)	11.1 (10.9 ± 0.5)

^a Data and statistics based on five cells of each condition.

^b Numbers in bold are the champion values of each condition.

ratio can be well addressed. It is worth noting that we ignore the impact of heavy doping on optical absorption, which means the same optical performances under different doping concentrations as shown in Fig. 3b. Besides, the photoelectric parameters of silicon used in the simulation, including refractive index, electron and hole mobility, carrier lifetime, coefficients of carrier recombination, material bandgap, etc., can be found in previous publications [28–30].

4.2. Fabrication of micropillar arrays

Czochralski grown, 400- μm -thick, double-side polished *p*-type (100) Si wafers (2–4 $\Omega\text{ cm}$) were utilized in the work. The micropillar arrays were fabricated via an anisotropic wet etching technique, as introduced elsewhere [31,32]. Monodispersed polystyrene (PS) microspheres with two different pitches (1.2 μm and 2.4 μm) were separately assembled on the Si substrate via Langmuir-Blodgett (LB) method, followed by a reactive-ion etching (RIE) operation to reduce the diameter of microspheres [33,34]. A 1.5/5/10 nm-thick Ti/Ag/Au metal catalyst was deposited by electron beam evaporation on the side covered with the microspheres [35].¹ After the removal of the PS microspheres with sonication in chloroform, the samples were covered through a shallow mask [36]. Another Ti/Au (1.5/20 nm) films were deposited on the gap of mask. The samples were immersed in a composited solution ($\text{H}_2\text{O}_2/\text{HF}/\text{H}_2\text{O}/\text{ktOH} = 1/5/10/10$ by volume) at room temperature for different time to control the height. Then the micropillar arrays were rinsed with aqua regia to remove Au mesh.

4.3. Fabrication of micropencil arrays

The micropencil arrays were made by a multiple-cycle chemical etching process [15]. The micropillar arrays were etched in a mixed solution of AgNO_3 (0.0002 M), HF (2 M) and HNO_3 (0.005 M) for 10–15 min. After every etching cycle, the samples were transferred into a 10 wt% HNO_3 solution for 2 min to remove the residual Ag clusters followed with a rinse in DI water.

4.4. Fabrication of silicon solar cells

The emitter layer was formed by the spin-on dopant (SOD) method. After the RCA cleaning (as developed at Radio Corporation of America), the phosphorus dopant source (P509, Filmtronics, Inc) was spin-coated on a dummy wafer, and then baked at 200 °C for 15–20 min. In order to tune the doping profiles, the diffusion temperature was varied from 800 °C to 950 °C for different batches. For each batch, a two-step diffusion process was conducted in a tube furnace under a mixed ambient atmosphere of O_2 (375 sccm) and N_2 (1125 sccm) for 30 min, followed with O_2 (1500 sccm) for 10 min. The reason of adding the second step is to oxidize the phosphorus-rich layer (PRL), so as to easily remove it by the following HF treatment. Removing the PRL can help to improve the passivation quality of sequentially coated passivation layer. The textured Si samples were abutted the dummy wafer for conformal doping. The phosphorous silicate glass which remained after SOD diffusion was removed by 4 vol% HF solution. A thin SiO_2 passivation layer was formed by thermal oxidation at 800 °C for 30 min. The thickness of SiO_2 layer is in the range of 5–15 nm depending on the amount of doped phosphorus that was controlled by the diffusion temperature. Back metal contact was made by aluminum paste and alloying at 750 °C. For the front metal contact, the grid pattern was formed by photolithography and etched in buffered hydrogen fluoride corrosion solution [37]. A Cr/Pd/Ag contact grid was made by electron beam evaporation and metal lift-off operation.

4.5. Characterization

The morphologies of the samples were conducted by scanning electron microscope (SEM, Zeiss Ultra Plus). Effective carrier lifetime

was analyzed by a microwave photoconductivity decay system (WCT-120, Sinton Consulting). The dopant concentration and junction depth were measured by electrochemical capacitance-voltage (ECV). The PV performance of solar cells was measured under a simulated AM 1.5 spectrum sunlight illumination and with a 0.5 cm^2 effective illumination area through a measurement mask. The reflectance and IQE curves were measured by a quantum efficiency system (QEX10).

Acknowledgments

This work was supported by the Major State Basic Research Development Program of China (No. 2018YFB1500302 and 2016YFB0700700), National Natural Science Foundation of China (11674225, 11834011, 11474201, 61674154, and 61874177), Natural Science Foundation of Zhejiang Province (LR19E020001, LR16F040002). We would like to thank Advanced Electronic Materials and Devices (AEMD) of Shanghai Jiao Tong University for supplying the facility of reactive-ion etching (RIE), Zhiwen Shi of Shanghai Jiao Tong University for supplying the software of COMSOL Multiphysics, as well as Yuheng Zeng of Ningbo Institute of Material Technology and Engineering for scientific support.

Appendix A. Supporting information

Supplementary data associated with this article can be found in the online version at doi:10.1016/j.nanoen.2019.02.021.

References

- [1] X. Liu, P.R. Coxon, M. Peters, B. Hoex, J.M. Cole, D.J. Fray, Energy Environ. Sci. 7 (2014) 3223–3263.
- [2] P. Yu, J. Wu, S.T. Liu, J. Xiong, C. Jagadish, Z.M.M. Wang, Nano Today 11 (2016) 704–737.
- [3] S. Zhong, Z. Huang, X. Lin, Y. Zeng, Y. Ma, W. Shen, Adv. Mater. 27 (2015) 555–561.
- [4] Z. Huang, X. Song, S. Zhong, H. Xu, W. Luo, X. Zhu, W. Shen, Adv. Funct. Mater. 26 (2016) 1892–1898.
- [5] J. Oh, H.C. Yuan, H.M. Branz, Nat. Nanotechnol. 7 (2012) 743–748.
- [6] J. He, P. Gao, M. Liao, X. Yang, Z. Ying, S. Zhou, J. Ye, Y. Cui, Acs Nano 9 (2015) 6522–6531.
- [7] H. Savin, P. Repo, G.G. Von, P. Ortega, E. Calle, M. Garín, R. Alcubilla, Nat. Nanotechnol. 10 (2015) 624.
- [8] I. Hwang, H.-D. Um, B.-S. Kim, M. Wober, K. Seo, Energy Environ. Sci. 11 (2018) 641–647.
- [9] J. Liu, X. Zhang, G. Dong, Y. Liao, B. Wang, T. Zhang, F. Yi, Appl. Surf. Sci. 289 (2014) 300–305.
- [10] K. Lee, I. Hwang, N. Kim, D. Choi, H.D. Um, S. Kim, K. Seo, Nanoscale 8 (2016) 14473–14479.
- [11] J.Y. Jung, Z. Guo, S.W. Jee, H.D. Um, K.T. Park, M.S. Hyun, J.M. Yang, J.H. Lee, Nanotechnology 21 (2010) 445303.
- [12] A.S. Togonol, M. Foldyna, W. Chen, J.X. Wang, V. Neplokh, M. Tchernycheva, J. Nassar, P.R.J. Cabarrocas, Rusli, J. Phys. Chem. C 120 (2016) 2962.
- [13] S.A. Lee, T.H. Lee, C. Kim, M.G. Lee, M.-J. Choi, H. Park, S. Choi, J. Oh, H.W. Jang, ACS Catal. 8 (2018) 7261–7269.
- [14] B. Zhou, X. Kong, S. Vanka, S. Chu, P. Ghamari, Y. Wang, N. Pant, I. Shih, H. Guo, Z. Mi, Nat. Commun. 9 (2018) 3856.
- [15] H. Lin, H.Y. Cheung, F. Xiu, F. Wang, S.P. Yip, N. Han, T.F. Hung, J. Zhou, J.C. Ho, C.Y. Wong, J. Mater. Chem. A 1 (2013) 9942–9946.
- [16] H. Lin, F. Xiu, M. Fang, S. Yip, H.Y. Cheung, F. Wang, N. Han, K.S. Chan, C.Y. Wong, J.C. Ho, ACS Nano 8 (2014) 3752–3760.
- [17] X. Liang, L. Shu, H. Lin, M. Fang, H. Zhang, G. Dong, S. Yip, F. Xiu, J.C. Ho, Sci. Rep. 6 (2016) 34139.
- [18] K. Lee, I. Hwang, N. Kim, D. Choi, H.D. Um, S. Kim, K. Seo, Nanoscale 8 (2016) 14473–14479.
- [19] J. He, Z. Yang, P. Liu, S. Wu, P. Gao, M. Wang, S. Zhou, X. Li, H. Cao, J. Ye, Adv. Energy Mater. 6 (2016) 1501793.
- [20] Z. Huang, S. Zhong, X. Hua, X. Lin, X. Kong, N. Dai, W. Shen, Prog. Photovolt. Res. Appl. 23 (2015) 20964–20972.
- [21] B.M. Kayes, H.A. Atwater, N.S. Lewis, J. Appl. Phys. 97 (2005) (610–149).
- [22] S. Wang, X. Yan, X. Zhang, J. Li, X. Ren, Nanoscale Res. Lett. 10 (2015) 22.
- [23] A. Richter, S.W. Glunz, F. Werner, J. Schmidt, A. Cuevas, PhRvB 86 (2012) 4172–4181.
- [24] P. Procé, A. Ingenito, R.D. Rose, S. Pierro, F. Crupi, M. Lanuzza, G. Cocorullo, O. Isabella, M. Zeman, Prog. Photovolt. Res. Appl. 25 (2017) 452.
- [25] A. Cuevas, P.A. Basore, G. Giroult-Matlakowski, C. Dubois, J. Appl. Phys. 80 (1996) 3370–3375.
- [26] P.C. Dhanasekaran, B.S.V. Gopalam, Solid State Electron. 24 (1981) 1077–1080.

- [27] Y.W. Ok, A. Rohatgi, Y.H. Kil, S.E. Park, D.H. Kim, J.S. Lee, C.J. Choi, IEDL 32 (2011) 351–353.
- [28] Z. Yang, X. Li, S. Wu, P. Gao, J. Ye, Opt. Lett. 40 (2015) 1077–1080.
- [29] Z. Yang, P. Gao, J. He, W. Chen, W.-Y. Yin, Y. Zeng, W. Guo, J. Ye, Y. Cui, ACS Energy Lett. 2 (2017) 556–562.
- [30] A. Shang, X. Li, Adv. Mater. 29 (2016) 1603492.
- [31] J.Y. Choi, T.L. Alford, C.B. Honsberg, Langmuir 31 (2015) 4018–4023.
- [32] K. Peng, A. Lu, R. Zhang, S.T. Lee, Adv. Funct. Mater. 18 (2010) 3026–3035.
- [33] P. Gao, J. He, S. Zhou, X. Yang, S. Li, J. Sheng, D. Wang, T. Yu, J. Ye, Y. Cui, Nano Lett. 15 (2015) 4591–4598.
- [34] X. Wang, Z. Yang, P. Gao, X. Yang, S. Zhou, D. Wang, M. Liao, P. Liu, Z. Liu, S. Wu, Opt. Express 25 (2017) 10464–10472.
- [35] S.M. Kim, D.Y. Kang, Small 10 (2014) 3761–3766.
- [36] H. Lin, M. Fang, H.Y. Cheung, F. Xiu, S. Yip, C.Y. Wong, J. Ho, RSC Adv. 4 (2014) 50081–50085.
- [37] J. Bullock, M. Hettick, J. Geissbühler, A.J. Ong, T. Allen, Carolin M. Sutter-Fella, T. Chen, H. Ota, E.W. Schaler, S. De Wolf, C. Ballif, A. Cuevas, A. Javey, Nat. Energy 1 (2016) 15031.



Fei Wu received the Bachelor degree in MinZu University of China, in 2016. She is currently a Master candidate in the School of Physics and Astronomy, Shanghai Jiao Tong University. Her research interests include solar energy materials and solar cells.



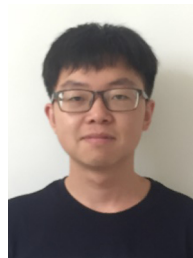
Hao Lin received his B.S. and M.S. degree in faculty of Science from Ningbo University, China, in 2010 and 2013, respectively. From 2012–2015, he worked in department of Physics and Materials Science, City University of Hong Kong. Currently, he is a Ph.D. candidate at School of Physics and Astronomy, Shanghai Jiao Tong University. His research interests include the solar energy materials, anti-reflection structure and dopant-free all-back-contact solar cells.



Zhenhai Yang is a joint training of Ph.D. student between the University of Nottingham Ningbo China and Ningbo Institute of Materials Technology and Engineering, Chinese Academy of Science. He received his B.Eng. degree in Optical Engineering from Huaiyin Normal University, Huai'an, China, in 2012, and master's degree in the School of Optoelectronic Information Science and Engineering, College of Physics from Soochow University, Suzhou, China, in 2015. His research interests focus on the heterojunction photoelectric devices and the advanced optical designs.



Mingdun Liao received the B.S. degree in microelectronics and the master's degree in condensed matter physics from Shandong University, Shandong, China, in 2006 and 2009, respectively. He is currently an engineer with the Ningbo Institute of Materials Technology & Engineering, Chinese Academy of Sciences, Ningbo, China. His current research interests include the novel crystalline silicon solar cell process towards industrial application.



Zilei Wang received his B.S. degree in College of Physics and Information Engineering at Fuzhou University, China, in 2015. He is involved in a joint program between University of Science and Technology of China and Ningbo Institute of Materials Technology and Engineering, Chinese Academy of Sciences (CAS) in Ningbo, China. His research interests focus on organic-inorganic hybrid solar cells.



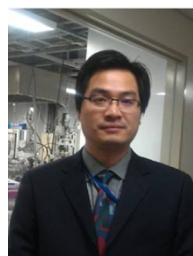
Zhengping Li received his Ph.D. degree in materials science and engineering from Shanghai Institute of Ceramics, Chinese Academy of Sciences, in 2003. From 2009–2011, he was a postdoctoral research fellow in the School of Physics and Astronomy, Shanghai Jiao Tong University, Shanghai, China, where he is currently an assistant professor of the Institute of Solar Energy. His research interests include solar energy materials and high-efficient solar cells.



Pingqi Gao received Ph.D. degrees in Department of Physics from Lanzhou University in 2010. From 2007–2011, he worked in Nanyang Technological University as a visiting researcher and a research staff. In 2013, he joined Ningbo Institute of Materials Technology and Engineering, CAS, as an associate professor and then a professor (2015). Since 2018, Dr. Gao has been with Sun Yat-sen University, China, as a full professor in the School of Materials. His research focus on high efficiency solar cell technology, especially on developing new materials and processes for solar energy conversion. He has published over 80 journal papers and serves as an active referee for 20 journals.



Jichuan Ye received the B. S. degree in Materials Science and Engineering from University of Science and Technology of China in 2001 and the Ph.D degree in Materials Science from University of California, Davis, USA in 2005. He joined Ningbo Institute of Material Technology and Engineering, CAS, as a professor and Ph.D. advisor since August of 2012. He was awarded for "Thousand Young Talents Program of China" in 2012. He has published more than 60 publications with nearly 500 times citations, applied more than 40 patents (including 10 awarded patents).



Wenzhong Shen received his Ph.D. degree in semiconductor physics and semiconductor device from Shanghai Institute of Technical Physics, Chinese Academy of Sciences, in 1995. Since 1999, Dr. Shen has been with Shanghai Jiao Tong University, China, as a full professor in the School of Physics and Astronomy, where he is currently the director of Institute of Solar Energy and Key Laboratory of Artificial Structures and Quantum Control, Ministry of Education.